Structure and Growth of Polymeric Niobia-Silica Mixed-Oxide Sols for Microporous Molecular Sieving Membranes: A SAXS Study

Vittorio Boffa,[†,‡] Hessel L. Castricum,[†,§] Ruben Garcia,[†] Riaan Schmuhl,[†] Andrei V. Petukhov,[||] Dave H. A. Blank,[†] and Johan E. ten Elshof*[,†]

MESA$^+$ Institute for Nanotechnology, University of Twente, P.O. Box 217, 7500 AE Enschede, The Netherlands, Van't Hoff Institute for Molecular Sciences, University of Amsterdam, Nieuwe Achtergracht 166, 1018 WV Amsterdam, The Netherlands, and Van't Hoff Laboratory for Physical and Colloid Chemistry Debye Research Institute, Utrecht University, Padualaan 8, 3584 CH Utrecht, The Netherlands

Received September 16, 2008. Revised Manuscript Received March 2, 2009

Branched polymeric niobia-silica (NS) mixed-oxide sols with a Nb:Si molar ratio between 0.33 and 0.8 were made by acid-catalyzed sol−gel synthesis and characterized using small-angle X-ray scattering (SAXS) and dynamic light scattering (DLS). The growth rate of NS sols after addition of a niobium alkoxide precursor to a prehydrolyzed silica sol in alcohol under highly acidic conditions was monitored. The results indicated a fractal structure, with radii of gyration and fractal dimensions that increased simultaneously as a function of time. The radii of gyration were between 2 and 5.5 nm, whereas the fractal dimensions were in the range of 1.5−2.0 within experimental error. The experimental data are indicative of growth via a diffusion-limited cluster aggregation (DLCA) mechanism on a time scale of hours. The dominant growth mechanism in the very early stage of reaction must have been different. Sols with higher Nb:Si molar ratios grew faster, which is due to the higher reactivity of Nb compared to Si alkoxides. Dilution and control over temperature can be employed to control the size of the sols precisely.

1. Introduction

Replacement of distillation and cryodistillation by membrane processes may lead to vast energy savings.[1,2] Molecular separation of biomass fuels[3] and hydrogen[4,5] via membranes could find use in upcoming technology platforms for green energy production. High gas separation selectivities have been obtained with microporous silica-based membrane materials. However, silica has inadequate thermal and hydrothermal stability to enable practical application.[6−8]

A strategy to stabilize microporous silica is to introduce transition metals in the silica network.[9−12] As oxygen forms more stable bonds with transition metals than with silicon, mixed oxide networks are more stable than amorphous silicon oxide. We recently developed a niobia-silica (NS) mixed oxide microporous membrane[13] that combines the open percolative pore structure of silica with increased thermal stability, and has a high selectivity for CO_2.[14] These NS membranes were made by depositing polymeric niobia-silica sols on an asymmetric support and annealing at 500 °C. The NS sols were synthesized by hydrolysis and condensation of Si and Nb alkoxides in alcohols, following the two fundamental reactions below

$$\text{Hydrolysis}\quad (R'O)_{n-1}M-OR + H_2O \xrightarrow{H^+} (R'O)_{n-1}M-OH + ROH$$

$$\text{Condensation}\quad (R'O)_{n-1}M-OH + HO-M(OR')_{n-1} \xrightarrow{H^+} (R'O)_{n-1}M-O-M(OR')_{n-1} + H_2O$$

Here, M is Nb or Si, R is an alkyl group, R′ are alkyl groups or M−O−M condensation polymers, and n is the oxidation state of the central M atom. In the first hydrolysis step, the precursor is activated by the formation of an OH group. In the following condensation reaction the formed M−OH groups are condensed into M−O−M bonds. After prolonged nucleation and growth, the resulting entities can be either

* Corresponding author. Phone: 31 53 489 2695. Fax: 31 53 489 3595. E-mail: j.e.tenelshof@utwente.nl.
† University of Twente.
‡ Present address: Dipartimento di Chimica Generale e Chimica Organica, Università di Torino, Corso M. D'Azeglio 48, 10125 Torino, Italy.
§ University of Amsterdam.
|| Utrecht University.

(1) Feng, X. S.; Huang, R. Y. M. *Ind. Eng. Chem. Res.* **1997**, *36*, 1048.
(2) Jonquieres, A.; Clement, R.; Lochon, P.; Neel, J.; Dresch, M.; Chretien, B. *J. Membr. Sci.* **2002**, *206*, 87.
(3) Vane, L. M. *J. Chem. Technol. Biotechnol.* **2005**, *80*, 603.
(4) Lin, H. Q.; Van Wagner, E.; Freeman, B. D.; Toy, L. G.; Gupta, R. P. *Science* **2006**, *311*, 639.
(5) Nenoff, T. M.; Spontak, R. J.; Aberg, C. M. *MRS Bull.* **2006**, *31*, 735.
(6) Himai, H.; Morimoto, H.; Tominaga, A.; Hiraschima, H. *J. Sol−Gel Sci. Technol.* **1997**, *10*, 45.
(7) Iler, R. K. *The Chemistry of Silica*; Wiley & Sons: New York, 1979.
(8) Tsapatsis, M.; Gavalas, G. *J. Membr. Sci.* **1994**, *87*, 281.
(9) Asaeda, M.; Sakou, Y.; Yang, J. H.; Shimasaki, K. *J. Membr. Sci.* **2002**, *209*, 163.
(10) Sekulic, J.; Luiten, M. W. J.; Ten Elshof, J. E.; Benes, N. E.; Keizer, K. *Desalination* **2002**, *148*, 19.
(11) Kanezashi, M.; Asaeda, M. *J. Chem. Eng. Jpn.* **2005**, *38*, 908.
(12) Liu, W.; Zhang, B. Q.; Liu, X, F.; Xu, L. M. *Chin. J. Chem. Eng.* **2006**, *14*, 31.
(13) Boffa, V.; Ten Elshof, J. E.; Petukhov, A. V.; Blank, D. H. A. *ChemSusChem* **2008**, *1*, 437.
(14) Boffa, V.; Blank, D. H. A.; Ten Elshof, J. E. *J. Membr. Sci.* **2008**, *319*, 256.

10.1021/cm802511w CCC: $40.75
Published on Web 04/07/2009

dissolved branched inorganic polymers with relatively low dimensionality or dense mixed-metal oxide-hydroxide nanoparticles dispersed in solution. The morphology depends on the type of metal used, and on the conditions during reaction.

A prerequisite to obtain a high-quality thin layer with molecular sieving selectivity is that the sol consists of building blocks that are slightly larger than the pore size of the underlying mesoporous support layer.[15,16] Furthermore, a microporous network with pore sizes $\ll 1$ nm can be formed only if the inorganic polymers are slightly branched. The degree of branching of a polymer can be expressed in terms of the fractal dimension parameter D_f, which relates the mass m and radius of gyration R_g of a polymer via

$$m \approx R_g^{D_f} \quad (1)$$

Nonbranched polymers typically have a fractal dimension D_f of 1, whereas dense spherical particles have $D_f = 3$. Branched polymers have a fractal dimension between these two extreme values. Mandelbrot demonstrated that fractal-like structures are mutually transparent, i.e., they can interpenetrate one another only if their fractal dimensions (D_f) are smaller than 1.5.[17] In reality, microporous silica membranes have been made from sols with higher D_f values, up to 1.7−1.8.[18] The discrepancy between theory and practice may be explained by the fact that not all collisions between branches result in bond formation,[18] and that the D_f value calculated from small-angle X-ray scattering (SAXS) spectra is some average of a distribution of inorganic polymers with varying radii of gyration and degrees of chain branching. Polymeric sols with a fractal dimension above ~2 are expected to result in mesoporous structures.[19] This is due to "hard sphere packing", and the pore sizes in such films are on the order of the sol size.[20]

Although polymeric silica sols have been studied by several authors and optimal process conditions have been defined for membrane preparation,[21−24] comparatively little is known about the structure and growth mechanism of metal-doped silicon oxide materials. In this study, we report the structural development of mixed Nb−Si oxide polymeric sols as a function of a number of processing parameters. We used SAXS and dynamic light scattering (DLS) experiments to investigate the reactivity of the precursors during the earliest stages of reaction, and the development of sols of which the structure meets all required conditions for membrane processing. The influence of pH, hydrolysis ratio, Nb:Si molar ratio, temperature, nature and size of the alkoxy group, and total metal alkoxide concentration are evaluated.

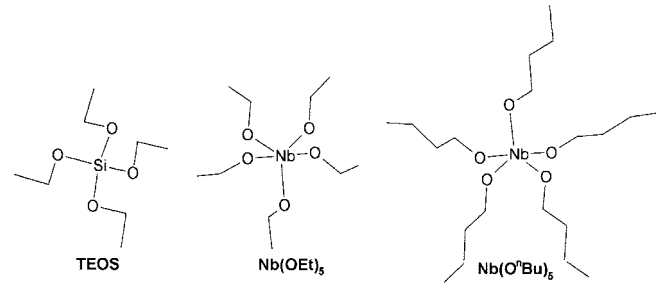

Figure 1. Chemical formulas of the metal oxide precursors used in the syntheses.

Table 1. Preparation Parameters of Sols (ratios r_W, r_H, and r_S are defined in eqs 2−4)

sol	Nb: Si molar ratio	r_W	r_H	r_S	T (°C)	Nb precursor
A	0	1	0.05	10	60	
A1	0.80	0.5	0.025	6.3	60	$Nb(OEt)_5$
A2	0.80	0.5	0.025	6.3	80	$Nb(OEt)_5$
A3	0.80	0.5	0.025	5.6	60	$Nb(O^nBu)_5$
A4	0.80	0.5	0.025	36	60	$Nb(OEt)_5$
B	0	0.7	0.35	10	60	
B1	0.33	0.5	0.025	7.8	60	$Nb(OEt)_5$
B2	0.33	0.7	0.025	7.8	60	$Nb(OEt)_5$
B3	0.33	0.7	0.1	7.8	60	$Nb(OEt)_5$
C	0	0.5	0.01	1	60	
C1	0.33	0.5	0.01	1	60	$Nb(OEt)_5$
C2	0.33	0.5	0.01	1	60	$Nb(O^nBu)_5$

2. Experimental Section

2.1. Reagents. The metal oxide precursors used in this study are depicted in Figure 1. Tetraethyl orthosilicate (TEOS) was purchased from Aldrich with purities of 99.999%. Niobium(V) penta(*n*-butoxide) ($Nb(O^nBu)_5$), and niobium(V) penta(ethoxide) ($Nb(OEt)_5$) were purchased from Gelest. Nitric acid (65%), ethanol (99.8%) and 1-butanol (99.8%) were purchased from Aldrich. All solvents were anhydrous to control the water concentration in the system. Deionized water ($\rho = 18.2$ MΩ cm) was prepared using a TKA water purification unit.

2.2. Sample Preparation. Three series of NS sols were made following three different synthesis methods. Since the niobia alkoxides are more sensitive to hydrolysis and condensation than TEOS, the NS sols were prepared in a two-step synthesis method. In the first step, TEOS was prehydrolyzed at 60 °C for 2 h. One of the Nb alkoxide precursors was then added and reacted at 60 °C under reflux. Samples for SAXS analysis were collected after 0, 30, 90, 150, and 300 min of reaction time and thermally quenched. These samples are referred to following the designations listed in Table 1. The designation will be followed by the reaction time in minutes.

The A-type and B-type sols were prepared by adding all water and nitric acid at the beginning of the prehydrolysis stage. In the synthesis of C-type sols aqueous nitric acid was added in two steps, namely at the beginning of the prehydrolysis stage, and directly after the introduction of the Nb alkoxide precursor in the mixture.[13] The A-type sols have a higher Nb:Si molar ratio than the B- and C-type sols, whereas the C-type sols are more concentrated than the A- and B-type sols.

The growth of sol−gel silica-based structures is known to be kinetically controlled,[7] so that the morphology of the sols depends on many synthesis parameters, i.e., reaction time, temperature, and concentration of the metal oxide precursors, water, and acid. The

(15) De Vos, R. M.; Verweij, H. *J. Membr. Sci.* **1998**, *143*, 37.
(16) Uhlhorn, R. J. R.; Keizer, K.; Burggraaf, A. J. *J. Membr. Sci.* **1992**, *66*, 271.
(17) Mandelbrot, B. B. *The Fractal Geometry of Nature*; W. H. Freeman: New York, 1982.
(18) Brinker, C. J.; Ward, T. L.; Sehgal, R.; Raman, N. K.; Hietala, S. L.; Smith, D. M.; Hua, D.-W.; Headley, T. J. *J. Membr. Sci.* **1993**, *77*, 165.
(19) Brinker, C. J.; Scherer, G. W. *J. Non-Cryst. Solids* **1985**, *70*, 301.
(20) Kammler, H. K.; Beaucage, G.; Mueller, R.; Pratsinis, S. E. *Langmuir* **2004**, *20*, 1915.
(21) Brinker, C. J.; Frye, G. C.; Hurd, A. J.; Ashley, C. S. *Thin Solid Films* **1991**, *210*, 97.
(22) De Lange, R. S. A.; Hekkink, J. H. A.; Keizer, K.; Burggraaf, A. J. *J. Non-Cryst. Solids* **1995**, *191*, 1.
(23) Nair, B. N.; Elferink, W. J.; Keizer, K.; Verweij, H. *J. Colloids Interface Sci.* **1996**, *178*, 565.
(24) Meane, N.; Nair, B. N.; D'Hooghe, P.; Nakao, S.-I.; Keizer, K. *J. Sol−Gel Sci. Technol.* **1998**, *12*, 117.

relevant reaction parameters are listed in Table 1. The given water and acid concentrations are expressed in terms of hydrolysis ratio and acid ratio, as defined by eqs 2 and 3

$$r_W = \frac{[H_2O]}{\sum_i v_i[M_i]} \quad (2)$$

$$r_H = \frac{[H^+]}{\sum_i v_i[M_i]} \quad (3)$$

where $[H_2O]$, $[H^+]$, and $[M_i]$ indicate the concentrations of water, HNO_3, and metal (Nb or Si), and v represents the formal oxidation state of the metal ion (4 for Si, 5 for Nb). The r_S ratio, defined by eq 4, expresses the solvent-to-metal ratio and is proportional to the reciprocal of metal atom concentration

$$r_S = \frac{[S]}{\sum_i v_i[M_i]} \quad (4)$$

Here [S] is the concentration of solvent. All precursors were dissolved in their parent alcohols, i.e., metal ethoxides were dissolved in ethanol, and metal *n*-butoxides in *n*-butanol.

2.3. SAXS Experiments. Samples were placed in a capillary glass tube (∅ 1.5 mm, glass no. 14, Hildenberg, Malsfeld, Germany). Small-angle X-ray scattering were carried out using synchrotron radiation on the Dutch-Belgian DUBBLE beamline BM-26B of the ESRF in Grenoble, using a beam energy of 12 keV.[25] The beam was focused on a corner of the 2D CCD detector to maximize the range of accessible q values. By placing the 2D detector of DUBBLE at a distance of 1.5 m from the sample, the scattered intensity was measured for q (scattering vector) between 0.13 and 5.56 nm^{-1}. A beam stop was applied to shield the detector from the direct beam and to avoid saturation of the outgoing signal. The raw data were corrected for the pixel-dependent detector sensitivity and integrated for channels with the same q values. A background subtraction procedure was carried out using a capillary containing pure solvent and acquiring a scattering pattern under the same experimental conditions as the NS sols. After background subtraction, the fractal dimension D_f was determined from an exponential fit of the fractal region of the intensity scattering curve to[26]

$$I(q) \sim q^{-D_f} \quad (5)$$

For smaller q values (between 0.03 and 1.00 nm^{-1}) the detector was placed at 8 m from the sample and a second set of measurements was acquired at this distance. After a similar background subtraction procedure as above, the radius of gyration was determined by fitting eq 6 to the experimental data in a Guinier plot.[26]

$$I(q) \sim \exp\left(-q^2\frac{R_g^2}{3}\right) \quad (6)$$

2.4. Dynamic Light Scattering (DLS) Experiments. Mean sol size distributions of the freshly prepared sols were determined by dynamic light scattering (DLS) at 25 °C in a Malvern Zetasizer HS3000. A nominal 5 mW Helium Neon laser with 633 nm wavelength was used to measure the particle size distributions under angles of 12 and 90°. The correlograms were analyzed using the CONTIN method.[27]

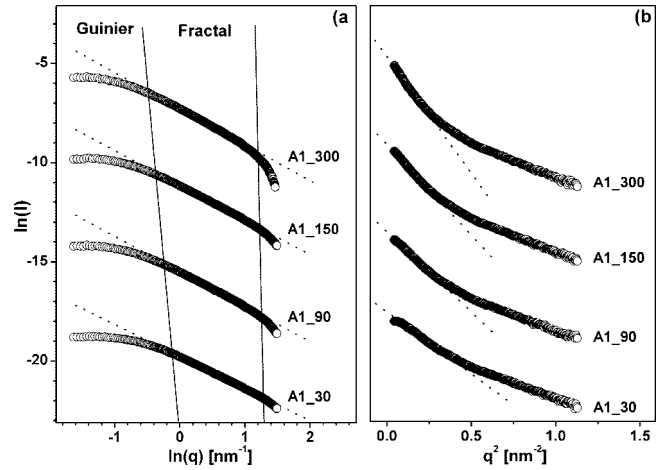

Figure 2. Scattering curves of sol A1, as monitored by SAXS. (a) In the Porod plot, the experimental data (detector-sample distance ≈ 1.5 m) were fitted to eq 5 (dotted lines). Every subsequent curve was displaced vertically by a factor of 50 for the sake of clarity. The vertical black lines were added as a guide to the eye to distinguish the Guinier and fractal regions in the graph, respectively. (b) In the Guinier plot, the experimental data (detector-sample distance ≈ 8 m) were fitted to eq 6.

Table 2. Evolution of Sol A1 with Time, As Determined from SAXS[a]

time(min)	D_f	r_0(nm)	ξ (nm)	R_g (nm)
30	1.60 ± 0.07	0.21	2.04	2.6 ± 0.1
90	1.73 ± 0.11	0.23	2.24	3.0 ± 0.1
150	1.72 ± 0.09	0.23	2.29	3.4 ± 0.1
300	1.81 ± 0.12	0.27	2.35	3.9 ± 0.1

[a] Fractal dimension (D_f), primary particle radius (r_0), and parameter ξ were calculated from the Porod plot in Figure 2a. The gyration radius R_g was calculated by fitting eq 6 to the Guinier plots of Figure 2b.

3. Results and Discussion

3.1. Structure of NS Sols by SAXS. The silica sols, A, B, and C were found to scatter only weakly, and the signal/noise ratio was too low to allow analysis of the SAXS spectra. This is typical for solutions containing poorly developed sols. However, the result was in agreement with our strategy, namely that in order to optimize the conditions for the formation of a homogeneous material, the concentration of (Si)−OH groups in the solution should be as high as possible at the moment that the niobia precursor is introduced into the reaction mixture. It is therefore desirable to avoid condensation among hydrolyzed species present in the solution during the prehydrolysis stage. The SAXS data confirm that condensation of silica in the prehydrolysis stage was limited or absent.

3.1.1. Fractal Dimension. In experiments with developed sols, substantial scattering was observed. The contribution of the background to the total signal was typically about 5% at low q, and 30−35% at high q. The evolution of sol A1 with time as determined by SAXS is shown in Figure 2 and Table 2. Figure 2a shows the Porod plot of the scattering curve. Equation 5 was used to fit the part of the graph indicated as "fractal region". The two thresholds of this

(25) Bras, W.; Dolbnya, I. P.; Detollenaere, D.; Van Tol, R.; Malfois, M.; Greaves, G. N.; Ryan, A. J.; Heeley, E. *J. Appl. Crystallogr.* **2003**, *36*, 791.
(26) Roe, R. J. *Methods of X-ray and Neutron Scattering in Polymer Science*; Oxford University Press: New York, 2000.
(27) Provencher, S. W. *Biophys. J.* **1976**, *16*, 27.

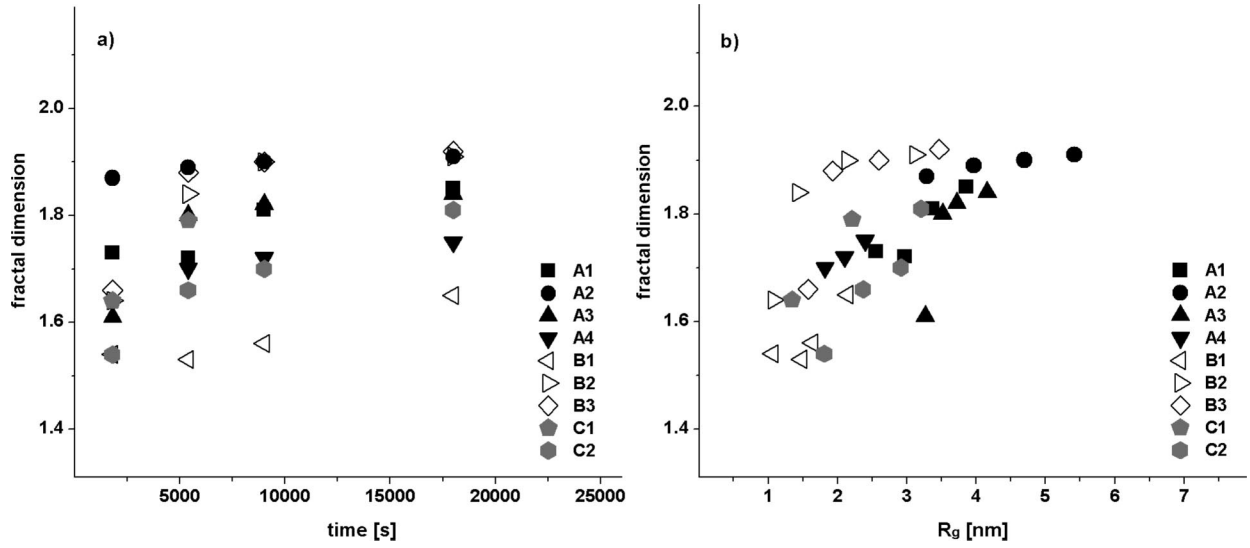

Figure 3. (a) Evolution of the fractal dimension (D_f) with time for various samples. (b) Fractal dimension D_f of all NS sols as function the gyration radius R_g.

region, $1/\xi$ and $1/r_0$ represent the reciprocal values of the correlation length of self-similar behavior ξ, and what is termed the radius of individual scatterers r_0.[28] The radius of gyration R_g is directly related to ξ.[29] The thresholds were calculated by determining the q values where the following criterion was no longer met

$$\left(\frac{\ln(I)_{exp} - \ln(I)_{fit}}{\ln(I)_{exp}}\right)^2 < 0.001 \quad (7)$$

Here $\ln(I)_{exp}$ is the natural logarithm of the scattered intensity as experimentally measured (white circles in Figure 2a) and $\ln(I)_{fit}$ is the corresponding value as calculated from the linear fit (dotted lines in Figure 2a). The locations of $1/r_0$ and $1/\xi$ are indicated by the black vertical lines. These lines have no physical meaning, but serve as a guide to the eye. Between 30 and 300 min of reaction time, the fractal dimension was seen to increase slightly, from 1.60 ± 0.07 to 1.81 ± 0.12. This rather modest increase was typical for all samples, as shown in Figure 3a.

The value of r_0, which is associated with the radii of the primary scatterers, of A1_30, A1_90, and A1_150 hardly change with time and are typically 0.21−0.23 nm. These values are similar to those reported by De Lange for silica[22] and by Sekulic et al. for amorphous titania.[29] For A1_300, a slightly larger r_0 of 0.27 nm was calculated from the data, which may be due to the low intensity of the signal at high q. The position of $1/\xi$ shifted toward lower q when reaction time increased. The increase of correlation length ξ is a direct consequence of particle growth.

All investigated NS sols had D_f values between 1.5 and 1.9, which is higher than TEOS based polymeric silica sols with typical D_f values between 1 and 1.5 under acid-catalyzed conditions.[22−24] The presence of a lowest fractal dimension of ∼1.5 can probably be attributed to Nb-alkoxides. Because of their high reactivity and coordination number than in Si-alkoxides, Nb precursors probably start forming inorganic polymers with a definite nonlinear shape in very early stages of synthesis, leading to more highly branched structures than Si alkoxides form. We showed in another study that microporous niobia-silica membranes could be prepared from A3_90, C2_90, and C2_300 sols.[30] These sols had D_f values varying between 1.66 and 1.87, and their radii of gyration varied between 2.4 and 4.0 nm.

3.1.2. Particle Size and Growth Mechanism. The radii of gyration R_g of the four sols A1 were determined from Guinier plots by fitting eq 6 to the data acquired at the longest detector-sample distance, in the q range between 0.05 and 0.15 nm^{-1}. The Guinier plots of sol A1, including the fits, are shown in Figure 2b. The R_g of sol A1 increased from 2.6 ± 0.1 nm after 30 min to 3.9 ± 0.1 nm after 300 min of reaction time.

The R_g values of type A, B, and C sols with corresponding D_f values are shown in Figure 3b. The two parameters were calculated independently but a rough correlation between them can be seen. In general, the radius of gyration and fractal dimension seem to increase simultaneously. However, for sols larger than $R_g \approx 4$ nm, the fractal dimension seems to reach an upper limit equal to 1.8−1.9. Because the error in the determination of D_f is about 0.07−0.10 for almost all experiments, and less than 0.15 for all, this suggests that $D_f < 2$ within experimental error.

The existence of an upper limit to D_f was also observed by Meane et al.[24] for polymeric silica, and by Peterlik et al.[31] for silica−alumina. They interpreted these data by assuming a growth mechanism that is dominated by diffusion-limited cluster aggregation (DLCA).[32,33] DLCA is a mechanism in which both monomer−cluster and cluster−cluster aggregation occur, and computer simulations have

(28) Teixeira, J. Experimental methods for studying fractal aggregates. In On Growth and Form; Tanley, H. E.; Ostrowsky, N., Eds; Martinus Nijhof: Dordrecht, The Netherlands, 1986; pp 145−162.
(29) Sekulić, J.; Ten Elshof, J. E.; Blank, D. H. A. *Adv. Mater.* **2004**, *16*, 1546.
(30) Boffa, V.; Garcia, R.; Blank, D. H. A.; Ten Elshof, J. E. *Microporous Mesoporous Mater.* **2009**, *118*, 202.
(31) Peterlik, H.; Rennhofer, H.; Torma, V.; Bauer, U.; Puchberger, M.; Hüsing, N.; Bernstorff, S.; Schubert, U. *J. Non-Cryst. Solids* **2007**, *353*, 1635.
(32) Meakin, P. *Phys. Rev. Lett.* **1983**, *51*, 1119.
(33) Kolb, M.; Botet, R.; Jullien, R. *Phys. Rev. Lett.* **1983**, *51*, 1123.

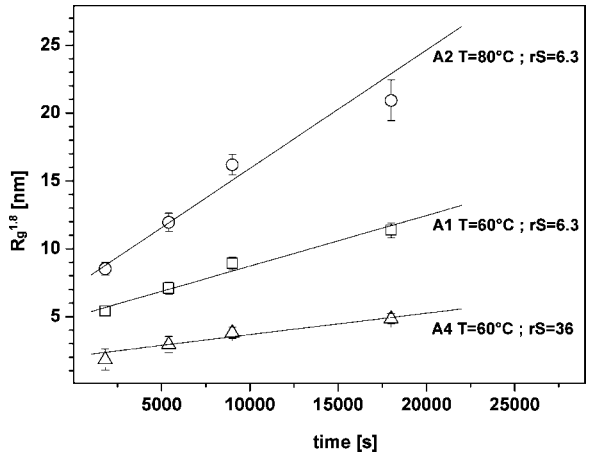

Figure 4. Evolution of the radius of gyration of sols A1, A2, and A4 with time, fitted following a $R_g^{1.8}$ dependency as predicted by the DLCA model (eq 8).

shown that this mechanism leads to fractal-like structures with a fractal dimension $D_f = 1.85 \pm 0.1$.[34,35] These simulations also showed that under DLCA conditions, the weight increase of a growing inorganic polymer dm is proportional to the time of growth dt, i.e., dm $\approx$ dt. Upon substitution of eq 1 and integration, it follows that

$$R_g^{D_f} - R_{g,0}^{D_f} = k_D t \tag{8}$$

where R_g is the radius of gyration at t seconds after introduction of niobium, and D_f the corresponding fractal dimension; $R_{g,0}$ is the radius of gyration of the silica sol at $t = 0$, and k_D represents a proportionality constant. Fitting the R_g values of several A-type sols to eq 8 while adopting $D_f = 1.8$ led to a good agreement between DLCA model and experimental data, as illustrated in Figure 4. It should be noted that equally good fits could also be made when D_f in Equation 8 was given any value in the range 1.6−2.0. Hence, the agreement between our experimental data and eq 8 does not exclude the possibility that the growth rate might be dominated by a process with power-law like behavior other than DLCA. However, the fact that $D_f < 2$ for virtually all sols is in accordance with DLCA, and excludes several other possible growth mechanisms. We therefore think that the DLCA mechanism provides the most likely explanation for our current data. Moreover, diffusion-controlled growth has also been reported for acid-catalyzed silica polymers by Nair et al.,[23] and for Ti- and Zr-doped silica polymers by De Lange et al.[22]

Since the particle growth rates of all sols presented in this work fit well to eq 8, calculated values of k_D can be used as a parameters to quantitatively compare the growth rates of NS sols under different synthesis conditions, regardless of the actual mechanism. Assuming that DLCA is dominant, the magnitude of k_D will depend on the molar volume of the metal oxide sols, and on their diffusion coefficients. In reality, the sol−gel reactions of silicon and niobium precursors are a complex process in which hydrolysis and condensation of numerous species occur simultaneously, generating new condensed reactive species in the entire course of reaction.

(34) Lin, M. Y.; Lindsay, H. M.; Weitz, D. A.; Ball, R. C.; Klein, R.; Meakin, P. *Proc. R. Soc. London, Ser. A* **1989**, *423*, 71.
(35) Meakin, P. *J. Sol−Gel Sci. Technol.* **1999**, *15*, 97.

Table 3. Fitted Parameters of Eq 8, Calculated from Experimental R_g Values of All Sols

sol	k_D ($m^{1.8}$ s^{-1})	$R_{g,0}$ (nm)
A1	$(2.3 \pm 0.3) \times 10^{-20}$	2.4 ± 0.1
A2	$(5.5 \pm 0.8) \times 10^{-20}$	2.0 ± 0.2
A3	$(1.8 \pm 0.1) \times 10^{-20}$	3.2 ± 0.1
A4	$(1.0 \pm 0.2) \times 10^{-20}$	1.5 ± 0.1
B1	$(1.1 \pm 0.1) \times 10^{-20}$	0.9 ± 0.1
B2	$(2.6 \pm 0.1) \times 10^{-20}$	0.6 ± 0.1
B3	$(2.8 \pm 0.1) \times 10^{-20}$	1.3 ± 0.1
C1	$(4.3 \pm 0.2) \times 10^{-20}$	0.7 ± 0.1
C2	$(3.4 \pm 0.3) \times 10^{-20}$	1.4 ± 0.1

Fitted parameters k_D and $R_{g,0}$ of all NS sols are listed in Table 3, where it was assumed that $D_f = 1.8$. The $R_{g,0}$ values were calculated by extrapolation to $t = 0$. Extrapolation is known to yield relatively large systematic errors. Yet the B- and C-type sols had comparatively similar $R_{g,0}$ values of 1.0 $\pm$ 0.4 nm. On the other hand, the $R_{g,0}$ values of the Nb-rich A-type sols varied clearly, with $R_{g,0}$ between 3.2 and 1.5 nm. These differences seem to be too large to be explained solely on the basis of extrapolation errors. They indicate that the growth rate of A-type sols in the early stage after addition of niobium precursor varied between samples. More importantly, they suggest that the growth rate in those early stages must have been higher than in the later quasi-steady state stages where DLCA was the dominant growth mechanism. Since the precursor concentration is highest at $t = 0$, when Nb precursor is added to the prehydrolyzed silica precursor solution, it is imaginable that a short burst of growth occurs in a relatively short period after this moment. Because of the high reactant concentrations, diffusional limitations were probably not rate-determining at that stage. Similar phenomena probably occurred in the B- and C-type sols, but since the concentration of the reactive Nb precursor was 2.4 times smaller in those systems, the effect will have been much less pronounced.

3.2. Influence of Preparation Parameters on Particle Growth. *3.2.1. Temperature.* Sols A1 and A2 were prepared with the same molar composition, but refluxed at 60 and 80 °C, respectively. Corresponding growth rate constants k_D equal to $(2.3 \pm 0.3)\cdot10^{-20}$ $m^{1.8}\cdot s^{-1}$ and $(5.5 \pm 0.8)\cdot10^{-20}$ $m^{1.8}\cdot s^{-1}$ were obtained. Although these two values do not permit calculation of the temperature dependency of the diffusion parameter k_D, they indicate that the reaction temperature affects the kinetics of inorganic polymer growth strongly. An R_g value of 5.4 $\pm$ 0.2 nm was calculated for sol A2 after 300 min of reaction. The radius of gyration of sol A1 under otherwise similar conditions was 3.6 $\pm$ 0.1 nm, which is about one-third smaller than that of A2.

3.2.2. Metal Alkoxide Concentration. As indicated in Table 1, sol A4 and A1 have the same molar composition, except for the dilution ratio r_S, which was higher for sol A4. The k_D value of $(1.0 \pm 0.2) \times 10^{-20}$ $m^{1.8}$ s^{-1} of sol A4 was much lower than that of sol A1. The R_g of sol A4 after 300 min at 60 °C was also smaller than that of sol A1. So dilution affects the growth rate of sols substantially. As A1 and A4 were made in the same solvent and at the same temperature, the diffusion coefficient of the hydrolyzed species within the solvent remained constant. However, as the formation of sol A4 took place in a more dilute medium, the diffusional

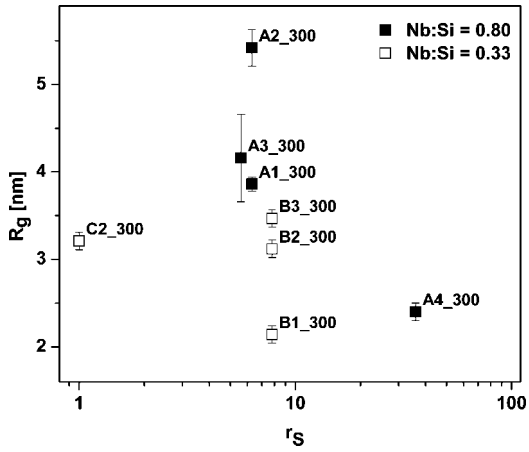

Figure 5. Gyration radius (R_g) of sols as function of the dilution ratio (r_S). Reflux time was 300 min at 60 °C.

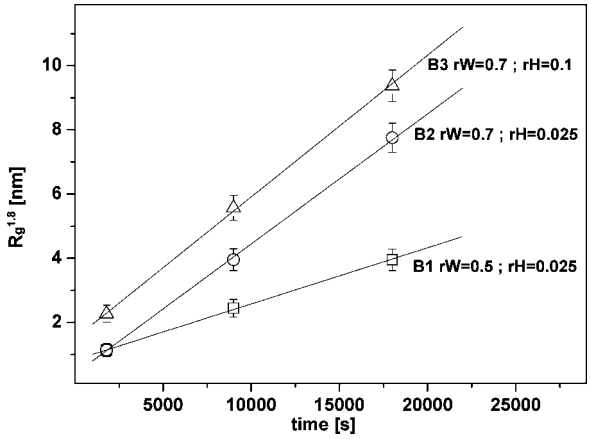

Figure 6. Evolution of the radius of gyration R_g of sols B1, B2, and B3 with time. The growth curve of each sol was fitted to eq 8.

supply of hydrolyzed species and thus the rate of condensation were smaller, resulting in smaller k_D and R_g values under otherwise similar conditions.

3.2.3. Composition. The radii of gyration after 300 min as a function of the dilution ratio r_S are shown in Figure 5. The results suggest that the evolution of R_g with time depends to a large extent on the Nb:Si molar ratio. Except for A4_300, which had a much higher dilution ratio than the others, the A-type sols (Nb:Si = 0.80) have larger R_g values than the sols prepared at a Nb:Si molar ratio equal to 0.33.

3.2.4. Hydrolysis Ratio r_w. Sol B2 was prepared at a higher hydrolysis ratio (r_W = 0.7) than B1 (r_W = 0.5). Their evolution is shown in Figure 6. The k_D values of B1 and B2 were $(1.1 \pm 0.1) \times 10^{-20}$ and $(2.6 \pm 0.1) \times 10^{-20}$ $m^{1.8}$ s^{-1}, respectively. The hydrolysis of two Si-OR bonds, followed by the formation of a Si−O−Si unit requires the net consumption of one water molecule. Thus, water is required for sol formation. Because the rate of hydrolysis of metal alkoxides is higher than the rate of condensation, and not all alkoxide side groups will be hydrolyzed under the conditions of the experiment (r_W < 1), increasing r_W leads to an effective increase of the concentration of hydrolyzed (OH-functional) species in solution that are able to undergo condensation. This explains the variation in k_D between B1 and B2. Attempts to prepare a niobia-silica sol at r_W = 0.25 yielded poorly developed sols, and their SAXS patterns had too low signal/noise ratios to permit data analysis. The higher hydrolysis ratio of sol B2 led to a higher concentration of Si-OH and Nb-OH groups, and therefore to a higher growth rate.

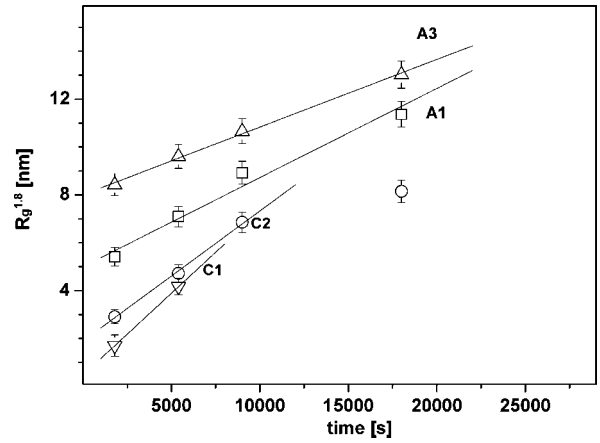

Figure 7. Evolution of the gyration radii R_g of sols A1, A3, C1, and C2 with time. The growth curve of each sol was fitted to eq 8.

Acidity Ratio r_H. All samples were prepared at high r_H. Such acid-catalyzed conditions are required to obtain branched and stable polymeric sols.[36] After 30 min the growth rate of B2 (r_H = 0.025) and B3 (r_H = 0.10) was similar, with a $k_D$of about 2.7×10^{-20} $m^{1.8}$ s^{-1}. However, B3 had an R_g of 1.54 ± 0.03 nm, whereas sol B2 had an R_g of about 1.1 nm. Thus, in the very first stages of reaction, the particle growth rate appears to have increased with increasing acid concentration.

Protons act as catalysts in both hydrolysis and condensation, increasing their respective rates. The results suggest that particle formation and growth in the early stages of reaction may have occurred under reaction-limited conditions.[23,37] After introduction of 1 M $Nb(OEt)_5$ at t = 0, a sol was formed by solvated silica-niobia polymers and hydrolyzed monomers in parallel. A solvent ratio r_S =7.8 corresponds to about 33 molecules of ethanol per atom of metal. Under such conditions it is unlikely that diffusion of hydrolyzed species is rate-determining, but the reaction rate between molecules could be. Nuclei will form very quickly, thereby decreasing the concentration of hydrolyzed species substantially. At some point, the diffusion of monomers and polymers to these centers becomes rate-determining. Nair et al.[23] proposed a shift from a reaction-limited process to a diffusion limited process in the synthesis and aging of polymeric silica sols.

The fact that B1 and B2, which had similar r_H but different r_W, both had a gyration radius of about 1.1 ± 0.1 nm after 30 min, while R_g of B3 (with higher r_H) was clearly larger. This is consistent with the findings reported in section 3.1 and confirms the importance of r_H in the early stages of reaction.

Nature of Niobium Precursor. Figure 7 shows the evolution of A1 and C1, which were both prepared using $Nb(OEt)_5$, and that of A3 and C2, which were made using

(36) Brinker, C. J.; Scherer, G. W. *Sol−Gel Science*; Harcourt Brace Jovanovich: Boston, MA, 1990.
(37) Cao, G. *Nanostructures & Nanomaterials−Synthesis, Properties and Applications*; Imperial College Press: London, 2004.

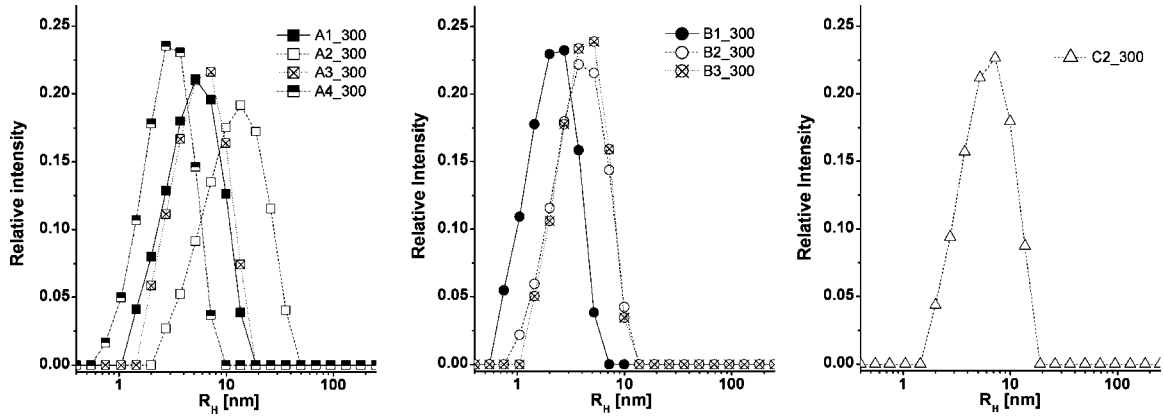

Figure 8. Size distribution of NS sols after 300 min of reaction, as determined by DLS.

Table 4. Mean Hydrodynamic Radius and Width of the DLS Distributions Shown in Figure 8

sol	$\langle R_H \rangle_I$ (nm)	fwhm (nm)	R_g (nm)
A1_300	5.5	8.5	3.9 ± 0.1
A2_300	9.8	23.3	5.4 ± 0.2
A3_300	6.3	9.6	4.2 ± 0.1
A4_300	3.1	4.2	2.4 ± 0.1
B1_300	2.3	3.2	2.1 ± 0.1
B2_300	4.3	6.2	3.1 ± 0.1
B3_300	4.4	6.0	3.5 ± 0.1
C2_300	7.6	7.6	3.2 ± 0.1

$Nb(O^nBu)_5$. Sol A3 had a smaller k_D than A1. A similar difference was observed when comparing sols C1 and C2. These differences could possibly be explained by the fact that an appreciable amount of 1-butanol was present in sols A3 and C2. Butanol was introduced together with $Nb(O^nBu)_5$, and was also formed upon hydrolysis of $Nb(O^nBu)_5$. 1-Butanol has a viscosity equal to 3.0 cP at 25 °C, which is almost three times higher than that of ethanol (1.074 cP). Hence the diffusion rate of niobia-silica polymers is probably somewhat slower in a butanol-containing solvent matrix, resulting in a smaller growth rate.

3.3. Size Polydispersity and Homogeneity of NS Sols. Information on sample polydispersity was obtained by dynamic light scattering (DLS) analysis. Although DLS provides less detailed and accurate information as SAXS does, it gives additional estimates on average hydrodynamic radius and width of the distribution, which can confirm the general trends observed by SAXS. Figure 8 shows the DLS-derived sol size distributions of NS sols after 300 min. Table 4 summarizes the intensity average hydrodynamic radii, $\langle R_H \rangle_I$, extrapolated from the distributions depicted in Figure 8, together with the full width at half-maximum (fwhm) of the distributions. The gyration radii of the sols in Table 4 are listed for the sake of comparison.

The data confirm the general trends in the SAXS data when temperature, r_W, r_H, or r_S were varied. In all cases the best fit to the data corresponded with a monomodal distribution of radii. The A-type sols, with a Nb:Si molar ratio of 0.80, had broader size distributions than the B- and C-type sols with a Nb:Si ratio of 0.33. The data also illustrate the importance of the Nb:Si ratio on particle growth rate. Sol A4_300 (Nb:Si = 0.8) had a slightly larger R_H than B1_300 (Nb:Si = 0.33), even though it had been prepared at a 4.6 times larger r_S value. Similarly, sol C2_300, which was prepared at $r_S = 1$, had a similar R_g as A3_300, though it had been prepared at a dilution ratio of $r_S = 5.3$. The higher Nb:Si ratio thus compensates the lower rate of condensation that is due to the higher r_S.

4. Conclusions

Branched polymeric niobia-silica mixed oxide sols made by a 2-step sol−gel synthesis procedure showed fractal dimensions D_f between 1.5 and 2.0 within experimental error. The fact that the fractal dimension was 1.8−1.9 in most samples is suggestive of growth by a DLCA mechanism, although our data do not exclude the possibility that another process could be active. DLCA-type growth has also been reported elsewhere for silica, and for Ti- and Zr-doped silicas. Higher growth rates were observed when the precursor concentration, Nb:Si molar ratio, and/or the reaction temperature were increased. Sols prepared at $r_W \leq 0.25$ were not well developed. Their scattering power in the SAXS experiments was too low to allow analysis of the data. Sols with $r_W = 0.5-0.7$ yielded stable polymeric sols with radii of gyration of 2−5.5 nm. The pH was found to influence particle growth in the earliest stages of reaction, and fitted $R_{g,0}$ values suggest a growth regime other than DLCA to be rate-determining in the initial stage of reaction after addition of niobium. A similar sequence of growth mechanisms was proposed by Nair et al. to explain the growth behavior of acid-catalyzed polymeric silica. The fractal dimensions of those silica systems was lower, i.e., 1.3−1.5,[23] than found in the present study.

Some of the sols studied in this work have been employed successfully elsewhere to prepare gas-selective microporous ceramic membranes.[30] The fractal dimensions of these sols varied between 1.66 ± 0.10 and 1.87 ± 0.15, and their radii of gyration varied between 2.4 and 4.0 nm. Apparently, this size is sufficiently small to allow complete interpenetration of sol polymers during film formation and sufficiently large to prevent penetration into the underlying mesoporous support.

Acknowledgment. Financial support from The Netherlands Technology Foundation (STW) is gratefully acknowledged. The authors thank the Dutch Organization for the Scientific Research (NWO) for the beam time to perform SAXS measurements at DUBBLE, and Kristina Kvashnina and Wim Bras (DUBBLE beamline) for on-site assistance.

CM802511W